Pergamon

Geochimica et Cosmochimica Acta, Vol. 67, No. 5, pp. 881–893, 2003

0016-7037/03 $30.00 + .00

PII S0016-7037(02)00957-2

Surface oxidation of pyrite under ambient atmospheric and aqueous (pH=2 to 10) conditions: Electronic structure and mineralogy from X-ray absorption spectroscopy

E. C. Todd,[1] D. M. Sherman,[1,*] and J. A. Purton[2]

[1]Department of Earth Sciences, University of Bristol, Bristol BS8 1RJ, UK
[2]Daresbury Laboratory, Warrington, UK

(*Received November* 19, 2001; *accepted in revised form May* 6, 2002)

Abstract—The nature of the surface oxidation phase on pyrite, FeS_2, reacted in aqueous electrolytes at pH = 2 to 10 and with air under ambient atmospheric conditions was studied using synchrotron-based oxygen K edge, sulfur L_{III} edge, and iron $L_{II,III}$ edge X-ray absorption spectroscopy. We demonstrate that O K edge X-ray absorption spectra provide a sensitive probe of sulfide surface oxidation that is complementary to X-ray photoelectron spectroscopy. Using total electron yield detection, the top 20 to 50 Å of the pyrite surface is characterized. In air, pyrite oxidizes to form predominantly ferric sulfate. In aqueous air-saturated solutions, the surface oxidation products of pyrite vary with pH, with a marked transition occurring around pH 4. Below pH = 4, a ferric (hydroxy)sulfate is the main oxidation product on the pyrite surface. At higher pH, we find iron(III) oxyhydroxide in addition to ferric (hydroxy)sulfate on the surface. Under the most alkaline conditions, the O K edge spectrum closely resembles that of goethite, FeOOH, and the surface is oxidized to the extent that no FeS_2 can be detected in the X-ray absorption spectra. In a 1.667×10^{-3} mol/L Fe^{3+} solution with ferric iron present as $FeCl_3$ in NaCl, the oxidation of pyrite is autocatalyzed, and formation of the surface iron(III) oxyhydroxide phase is promoted at low pH.

1. INTRODUCTION

1.1. Pyrite Oxidation

The surface oxidation of pyrite is the first stage in the development of acid mine drainage. Aqueous oxidation of pyrite releases H^+ ions, thiosulfate, tetrathionate, sulfite, and sulfate as well as dissolved iron into solution (Goldhaber, 1983; McKibben and Barnes, 1986; Moses et al., 1987; Xu and Schoonen, 1995).

Our interest here is in the chemical nature of the pyrite surface after oxidation. The nature of the oxidation layer on pyrite will determine the reactivity of weathered pyrite in aqueous solutions. In particular, the surface phase will determine how weathered pyrite might adsorb species such as $(AsO_4)^{3-}$. A surface oxide coating might even passivate against further oxidation of pyrite. On the basis of the change in aqueous oxidation products with time, it has been proposed that pyrite oxidation results in the formation of an Fe-hydroxide (Nicholson et al., 1988, 1990) or Fe-oxyhydroxide layer on the surface. Monosulfide, disulfide, and polysulfide have also been suggested as intermediate surface oxidation products, depending on the conditions and duration of oxidation (Hyland and Bancroft, 1989; Mycroft et al., 1990; Nesbitt and Muir, 1994; Pratesi and Cipriani, 2000). Electrokinetic studies have been performed on pyrite and other sulfides to investigate surface charge development as a function of pH and dissolved metal activity (Fornasiero et al., 1992; Dekkers and Schoonen, 1994; Bebie et al., 1998). The changes in surface charge are generally interpreted as resulting from the formation of a surface FeOOH layer.

* Author to whom correspondence should be addressed (Dave.Sherman@bristol.ac.uk).

1.2. X-Ray Photoelectron Studies

X-ray photoelectron spectroscopy (XPS) has been the primary technique used to provide a molecular characterization of the pyrite surface. Nesbitt and Muir (1994) and Nesbitt et al. (1998, 2000) characterized pristine fracture surfaces of pyrite under ultra–high vacuum. The reactivity of pyrite (100) and (111) planes to gaseous H_2O and O_2 was investigated by Guevremont et al. (1998b), and the surface oxidation of pyrite in air was studied by Eggleston et al. (1996) and Buckley and Woods (1987). Pratesi and Cipriani (2000) characterized the oxidation products with depth and found that the primary species produced by the oxidation of pyrite in air are sulfate and iron oxyhydroxides.

The surfaces of pyrite reacted with aqueous solutions were studied using XPS by Brion (1980), Mycroft et al. (1990), Karthe et al. (1993), Eggleston et al. (1996), and Bonnissel-Gissinger et al. (1998). Mycroft et al. (1990) found that oxidation creates a metal-deficient, S-rich surface in pyrite and other sulfides. This was supported by Bonnissel-Gissinger et al. (1998), who determined the surface oxidation products on pyrite reacted in aqueous solution as a function of pH (2 to 12). Below pH 4, they found that the pyrite surface contained 15% Fe(II) and Fe(III) (hydr)oxides and had an Fe-deficient composition $Fe_{1-x}S_2$. As the pH was raised, the amount of Fe(III) increased until above pH 10, all the surface iron consisted of an iron(III) (hydr)oxide. Although Bonnissel-Gissinger et al. (1998) found sulfate released into aqueous solution, they did not find evidence for sulfate on the pyrite surface.

1.3. X-Ray Absorption Spectroscopy

Unlike core-level XPS, X-ray absorption spectroscopy (XAS) measures the density of states of the unfilled (usually antibonding) electronic orbitals just above the Fermi energy.

This allows us to identify chemical bonds between atoms in addition to atomic valence states. For example, the O K edge spectrum results from excitation from the O (1s) core state to empty states with O (2p) character. The only empty states with O (2p) character will be those of atoms covalently bonded to the oxygen; hence, the O K edge spectra can be used to probe the Fe (3d) and S (3p) orbitals of compounds such as iron(III) oxyhydroxide, FeOOH, and ferric sulfate, $Fe_2(SO_4)_3$. Physisorbed H_2O on a mineral surface will not interfere with the O K edge spectrum because only the O-H antibonding orbitals are empty, and they are at a much higher energy than Fe-O and S-O antibonding orbitals. Also, under the ultra–high vacuum conditions of the X-ray absorption spectrometer, free water will be unstable at the mineral surface. A recent review of XAS of the near-edge region (referred to as NEXAFS by some authors) was given by Chen (1997). Previous X-ray absorption spectra of transition metal sulfides have largely focused on characterizing unoxidized bulk materials using the sulfur K and L edges. The S K edge and L edge features of bulk FeS_2 were studied by Sugiura (1981, 1984), Sugiura and Muramatsu (1985), and Li et al. (1995). The L edge features of pyrite and marcasite FeS_2 were assigned by Li et al. (1995). These studies have been useful in determining the oxidation state of sulfur in minerals and also in gaining information on their electronic structure, but as yet, XAS has not been used as a tool for identifying unknown species on mineral surfaces.

Using total electron yield (TEY) detection (as opposed to total fluorescence yield), we can obtain spectra of the top 20 to 50 Å of the pyrite surface (Abbate et al., 1992). Oxygen K edge spectra are particularly sensitive to any oxide or sulfate alteration product. The objectives of this paper, therefore, are to present a new approach to the examination of sulfide mineral surfaces, demonstrating the utility of XAS for characterization of both oxidation species and surface electronic structure. Our goals are to determine the nature of pyrite surfaces oxidized in air and air-saturated aqueous solutions as a function of pH and to use the quantitative information provided by the XAS technique to produce an electronic structure diagram for a complex oxidized pyrite surface.

2. EXPERIMENTAL METHODS

2.1. X-Ray Spectroscopy

The near-edge X-ray absorption spectra were measured at station 5U.1 of the Daresbury Synchrotron Radiation Source, England. An entrance-slitless, plane-grating, SX700-type monochromator was used (Mythen et al., 1992), with the exit slit set at 50 μm to give a high-energy resolution. Spectra were collected using the TEY method to measure the drain current. The mean probing depth in the TEY mode is 20 to 50 Å (Abbate et al., 1992), allowing analysis of the surface layers only. All data were recorded with the incident photon beam normal to the sample surface. The pressure in the sample chamber was less than 5×10^{-6} torr, and spectra were obtained at 25°C.

2.2. Sample Preparation

The pyrite specimens examined were natural samples from the University of Bristol's museum collection. Pyrite was characterized using X-ray diffraction and confirmed to be a single phase.

Three aqueous pyrite oxidation experiments were performed. The first set of pyrite samples were coarsely ground in a nitrogen glove box, then immersed in air-saturated 0.1 mol/L sodium nitrate solutions (pH = 2 to 5) for 5 d. The second and third sets of samples were pyrite single crystals. Pyrite slabs were coarsely polished under water in air and cleaned in a N_2 glove box by rinsing in 0.1 mol/L hydrochloric acid and deoxygenated milli-Q water. Samples were then immersed in an air-saturated 0.1 mol/L sodium chloride solution (pH = 3 to 10) for 4 d. The third set of samples was exposed to an additional 5×10^{-5} mol of $FeCl_3$. For all solutions, the pH was adjusted using 0.1 mol/L nitric acid or hydrochloric acid and 0.1 mol/L sodium hydroxide. (Note that the pH values given in the discussion below reflect the final pH. We assume that the solutions were never at equilibrium insofar as the oxidation of pyrite generates H^+). No attempt was made to exclude light during the aqueous oxidation experiments, on the basis of work by Xu and Schoonen (1995) that revealed that pyrite oxidation reactions in the dark and under normal laboratory illumination are indistinguishable. After conditioning, the samples were filtered and/or dried under N_2 and mounted on aluminum sample holders using carbon tape. A sample ground and stored in nitrogen was retained as a control. All procedures were carried out under nitrogen to ensure that the only oxidation products were those formed in aqueous solution. The samples were transferred rapidly to the spectrometer vacuum chamber to limit exposure to the atmosphere. We acknowledge the possibility that removing the pyrite samples from their solutions to characterize them may have changed their reacting surfaces; however, it is currently beyond the limitations of the XAS technique to perform aqueous measurements in situ. We consider that aqueous oxidation of the samples would passivate the pyrite surfaces to the extent that brief exposure to the atmosphere would have little effect on the oxidation products. This is confirmed by the systematic change in the surface composition with pH; i.e., the oxidation species present are intimately linked to the aqueous pH conditions. If the surfaces had equilibrated with air, we would expect uniformity across the sampling range.

The oxidation of pyrite in air was also studied. Pyrite was cleaved under nitrogen, then exposed to the ambient atmosphere (T = 20 C, $P_{H_2O} \sim 0.02$ bar) for 7 d. Goethite, γ-FeOOH, hematite, α-Fe_2O_3, and ferric sulfate, $Fe_2(SO_4)_3 \cdot 7H_2O$, references were included to assist in identification of oxidation products. These were synthetic, powdered samples and were characterized using X-ray diffraction. Sodium nitrate/chloride standards were also included for comparison. The standards were prepared for X-ray spectroscopy by finely grinding with ultrapure graphite, pressing into pellets, and mounting on the sample holders. All vacuum samples were handled with white gloves to ensure that the specimens remained grease free. Spectra were obtained in vacuo.

2.3. Data Collection and Calibration

We measured the oxygen K edge and iron L edge spectra of all samples and standards. For pyrite and ferric sulfate, we also measured the sulfur L edge. Nitrogen and chlorine spectra of the reacted pyrite surfaces were obtained to determine if electrolyte ions were adsorbing or precipitating on the mineral surface.

To correct for synchrotron intensity loss during measurement, the metal and sulfur L edge spectra were normalized by I/I_0, where I_0 is the intensity of the photon flux and I is the TEY. For the O K edges, the spectra were normalized to the photo-yield of clean gold mesh (sputtered until no oxygen edge was apparent). The spectra were aligned relative to each other using the peak positions in the internal reference spectra (the oxide coating on the reference mesh).

The O K edge spectra were resolved into constituent peaks by fitting to a set of gaussian functions on a constant baseline. We assigned the electronic transitions associated with these peaks (Table 1) by considering the known electronic structures of possible oxidized phases on the pyrite surfaces and by comparing the results to reference spectra of ferric sulfate, goethite, and hematite.

2.4. Raman Spectroscopy

Raman spectra of several of the pyrite samples were obtained with a DILOR X-Y spectrometer equipped with a charged-coupled-device detector and coupled to a confocal microscope. The spectral resolution was 3 cm^{-1}, with precision better than 1 cm^{-1}. The excitation line was the 514.5-nm emission from an argon ion laser source. The lateral spatial resolution was $\sim$1 μm, and the axial resolution was $\sim$3 μm. Laser power was typically 5 mW at the sample. Under the microscope, the reacted pyrite surfaces appear heterogeneous, with dark oxidized

Table 1. Peak assignments for O K edge spectra.

Peak	Average energy (eV)	Peak assignment
a	529.8	O (1s) in $O^{2-} \Rightarrow t_{2g}$ Fe (3d)–O (2p) antibonding molecular orbital in Fe_2O_3 and FeOOH
b	531.2	O (1s) in $O^{2-} \Rightarrow e_g$ Fe (3d)–O (2p) antibonding molecular orbital in Fe_2O_3 and FeOOH
c	532.2	O (1s) in $SO_4^{2-} \Rightarrow$ Fe (III) (3d) in a ferric (hydroxy)sulfate
d	532.6	O (1s) in $OH^- \Rightarrow$ Fe (III) (3d)
e	~534.0	Uncertain (multiple scattering resonance?)
f	537.2	O (1s) in $SO_4^{2-} \Rightarrow$ S (4s)–O (2p) antibonding molecular orbital in SO_4^{2-}
	539.0	O (1s) in $O^{2-} \Rightarrow$ Fe (4s, 4p)–O (2p) antibonding molecular orbital in Fe_2O_3 and FeOOH?
	542.0	O (1s) in $O^{2-} \Rightarrow$ Fe (4s, 4p)–O (2p) antibonding molecular orbital in Fe_2O_3 and FeOOH?
	547.0	Multiple scattering resonance
	557.0	Multiple scattering resonance

patches among bright, less oxidized regions. Raman spectra were taken of both areas.

3. RESULTS AND DISCUSSION

3.1. Electronic Structures and X-Ray Spectra of Iron (Oxyhydr)oxides, Sulfate, and FeS_2

To understand and interpret the X-ray absorption spectra of a complex oxidized sulfide surface, it is first necessary to consider the electronic structures and spectra of some single-phase oxide references. After assignment of the peaks in reference materials, it is possible to recognize characteristic features in the spectra of an unknown surface and hence to identify which species are present.

The electronic structures of iron(III) oxide and oxyhydroxide (e.g., Sherman, 1985a, 1985b) are shown schematically in Fig. 1. The lowest unoccupied levels correspond to the minority spin Fe (3d) levels. Above these are bands corresponding to the Fe (4s) and Fe (4p) atomic orbitals. The Fe (3d), Fe (4s), and Fe (4p) bands all contain appreciable O (2p) character attributable to the covalence of the Fe-O bond (Sherman, 1985a).

3.1.1. Oxygen K edge spectra

The oxygen K edge spectrum of hematite (Fig. 2a) results from transitions from the O (1s) core orbitals to the empty Fe (3d)–, Fe (4s)–, and Fe (4p)–like bands or molecular orbitals that have some O (2p) character. The crystal field splitting of the empty Fe (3d)–like orbitals can be resolved in the spectra (peaks a and b). For the iron(III) oxyhydroxide phase goethite (α-FeOOH), a more complex set of transitions to the unoccupied Fe (3d)–like orbitals is seen because transitions occur from both O (1s) (peaks a and b) and OH (1s) (peak d) core orbitals (Fig. 2b). The difference in energies between the O (1s) levels of O^{2-} and OH^- in goethite is approximately 1.4 eV. This is consistent with the values obtained by McIntyre and Zetaruk (1975) using XPS, which suggest a 1.6-eV energy difference between the binding energies of O (1s) electrons of O^{2-} in hematite and OH^- in goethite.

The oxygen K edge spectrum of ferric sulfate, $Fe_2(SO_4)_3 \cdot 7H_2O$ (Fig. 2c) shows a much weaker transition to the Fe (3d)–like orbitals (peak c), suggesting a smaller covalence of the Fe-O bond. Although iron is present in a trivalent state in this mineral, no ligand field splitting of the iron (3d) peak is seen. This may be a feature of the ionic nature of the Fe-O bond in ferric sulfate. Transitions to the Fe (3d) e_g-level, which has more O (2p) character than the corresponding t_{2g} level (Sherman, 1985a), may be strongly favored; hence, only

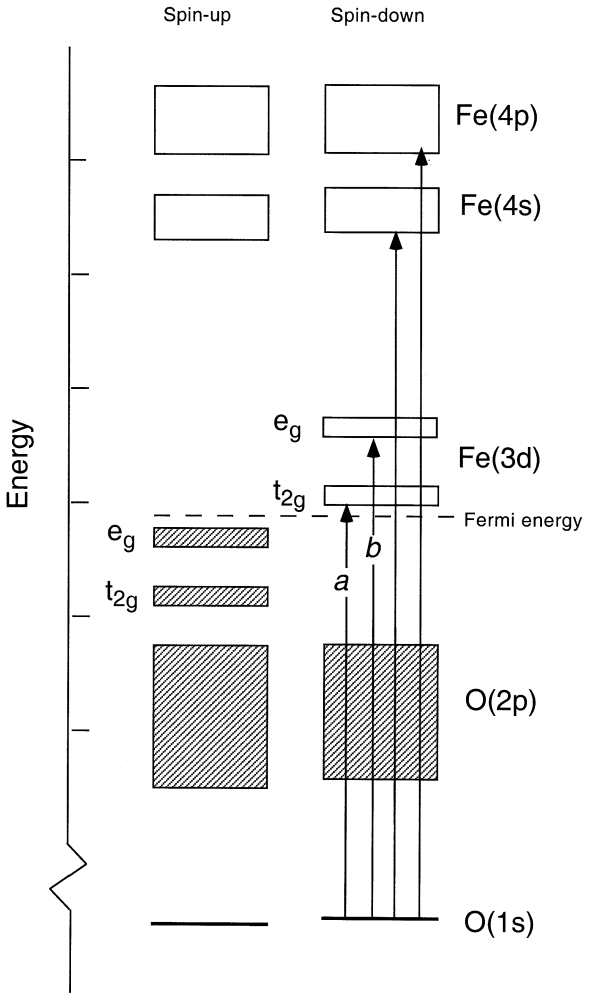

Fig. 1. The electronic structure of ferric oxides. The parity-allowed excitations give rise to peaks in the O K edge spectra of minerals such as hematite, α-Fe_2O_3, and goethite, γ-FeOOH.

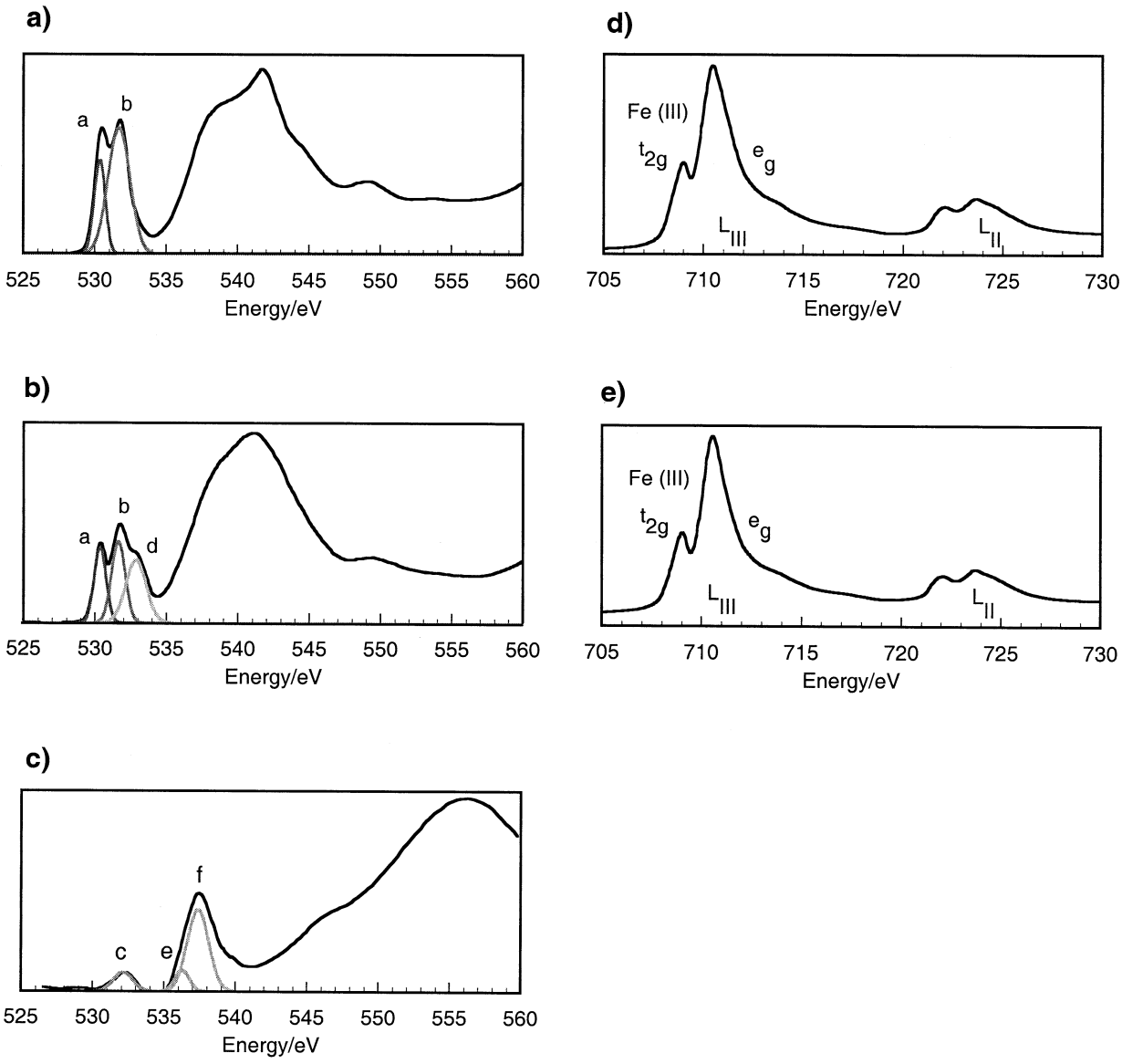

Fig. 2. (a) The oxygen K edge of hematite. The low-energy portion of the spectrum represents excitations from the O (2p) level to the t_{2g}- and e_g-like states of Fe (III) (peaks a and b). At higher energy, the peaks are attributed to excitations to the Fe (4s, 4p)–O (2p) molecular orbitals and to multiple scattering resonances. (b) The oxygen K edge of goethite. The low-energy portion of the spectrum is similar to that of hematite and again reflects the excitations from the O (2p) states to the t_{2g}- and e_g-like states of Fe (III) (peaks a and b). A third peak, c, represents excitations from the O (2p) level of oxygen in hydroxide to the Fe (3d)–like levels. (c) The oxygen K edge of ferric sulfate. The main peak, f, is assigned to transitions from the O (1s) to S (3p)–O (2p) antibonding orbital. Peak c is the O (1s) to Fe (3d)–O (2p) transition. (d) The iron L edge of iron oxide, hematite. The spectrum shows the characteristic splitting of the L_{III} and L_{II} edges, attributed to excitations from the Fe (III) (2p) states to Fe (III) t_{2g}- and e_g-like states. This is typical of iron (III) in octahedral coordination. (e) The iron L edge of iron oxyhydroxide, goethite. The spectrum is very similar to that of hematite and indicates the presence of Fe (III) in octahedral coordination.

one dominant peak will be observed in this region. Alternatively, the individual excitations to the t_{2g}- and e_g-like states may simply be unresolved. There is a single dominant peak at 537.5 eV (peak f), which we tentatively assign to transitions from the sulfate oxygen O (1s) to the S (3p,4s)–O (2p) antibonding orbitals.

Above 538 eV, the O K edge spectra are more difficult to interpret. This region contains the oxygen X-ray absorption near-edge spectrum. From the known electronic structure of the relevant minerals, the high-energy features are assigned generally to the Fe (4s)–O (2p) and Fe (4p)–O (2p) antibonding orbitals in the conduction band (e.g., Chen, 1997). In the region above 540 eV, the peaks are very broad and cannot be assigned excitations to any bound electronic states. It has been shown (Bianconi et al., 1982) that O^{2-} ions are strong back-scatterers and can give rise to barriers for electron scattering. On the basis of the multiple scattering calculations of Kurata et al. (1993), peaks in the region above 540 eV are described as multiple

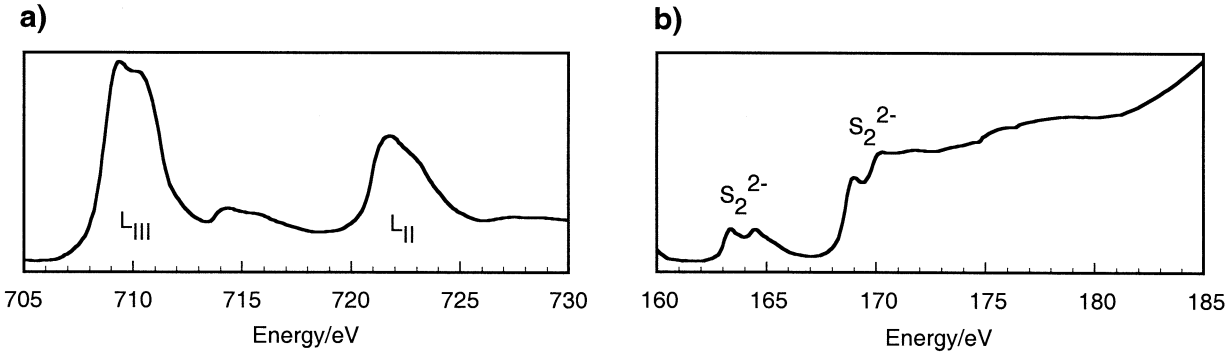

Fig. 3. (a) The iron L edge of pyrite ground under N_2. The spectrum represents excitations from the Fe (II) (2p) to Fe (II) (3d, 4s)–like states. The low L_{III}:L_{II} peak ratio suggests a low-spin Fe (II) electronic configuration for bulk pyrite. (b) The sulfur L edge of pyrite ground under N_2. The spectrum shows peaks attributed to excitations from the S (2p) to S_2^{2-} states, hybridized with Fe (II) (3d) states. The molecular S_2^{2-} ion is the dominant feature in the electronic structure of pyrite (Li et al, 1995).

scattering resonance features. Peak e, at approximately 534 eV, also cannot be assigned to an excitation to a bound state. It may be a multiple scattering feature, but its identity is uncertain.

3.1.2. Iron L edge spectra

The iron L edge spectra of goethite and hematite (Figs. 2d and 2e) result from transitions from the Fe (2p) core orbitals to the empty t_{2g}^{β} and e_g^{β} Fe (3d) orbitals and Fe (4s)–like valence band orbitals. The energy splitting between the t_{2g}^{β} and e_g^{β} Fe (3d)–like orbitals in the Fe L edge spectra is much greater than that determined from the oxygen K edge spectra. This presumably results from the greater orbital relaxation during the Fe (2p) to Fe (3d) transition. As discussed by de Groot et al. (1989), the $\Delta E(e_g\text{-}t_{2g})$ separations in the L edge are related but not equal to the crystal field-splitting energies, as would be determined from ligand field parameters derived from the optical spectra (e.g., Sherman and Waite, 1985). The O K edge features are much closer to the 10-Dq crystal-field splitting energies (de Groot et al., 1989).

The iron L edge spectrum of pyrite (Fig. 3a) results from transitions from the Fe (2p) core orbitals to the empty e_g Fe (3d) orbital. There should be no splitting of either the L_{III} or L_{II} edges for a pure pyrite surface. The Fe L edge spectrum of pyrite ground in N_2 (Fig. 3a), however, shows a slight splitting that must result from the presence of a small amount of Fe(III) on the pyrite surface, in addition to the bulk Fe(II). Nesbitt et al. (1998) proposed that ~40% of iron on a fractured pyrite surface is present as Fe(III) (one Fe[III] being produced for each S-S bond severed), and Nesbitt and Muir (1994) suggested that the observed proportions of S species on the oxidized surface can be explained if 20% of near-surface iron is Fe(III). This could explain the appearance of ferric iron on an unoxidized pyrite surface; however, the bulk of iron on the nominally unreacted pyrite surface is Fe(II).

In pyrite, iron is in the low-spin $(t_{2g})^6$ configuration of Fe(II), whereas iron in possible oxidation products such as FeOOH and $Fe_2(SO_4)_3$ is in the high spin $(t_{2g}^{\alpha})^3(e_g^{\alpha})^2$ configuration of Fe(III). This is seen in the Fe L edge L_{III}/L_{II} branching ratio, which is much lower for low-spin Fe(II) relative to that for high-spin Fe(II) or Fe(III) (Thole and Van der Laan, 1988). Bronold et al. (1994) proposed that low-spin iron in bulk pyrite could be converted to high spin at the {100} surface. The small L_{III}/L_{II} branching ratio for N_2-cleaved pyrite (Fig. 3a), however, is consistent with low-spin iron at the surface, supporting the ab initio calculations of Rosso et al (1999a), which showed no evidence for unpaired Fe (3d) electrons. The intensity ratio of the L_{III}/L_{II} features also depends strongly on the metal oxidation state. In general, the ratio is maximum at the d^5 configuration and decreases toward either d^0 or d^{10} (Sparrow et al., 1984). Hence, in the aqueous pyrite oxidation experiments, we might expect to see an increase in the L_{III}/L_{II} intensity ratio as the pH of the solutions increases and iron undergoes a transition from the low-spin (d^6) configuration of Fe^{2+} in FeS_2 to the high-spin (d^5) configuration in ferric oxidation products.

3.1.3. Sulfur L edge spectra

The sulfur L edge spectra of pyrite (Fig. 3b) and ferric sulfate result from transitions from the S (2p) core orbital to the empty conduction band orbitals that have some S (3d) and S (4s) character. The peaks of the S L edge are split by the spin-orbit interaction of S (2p) orbitals (Li et al., 1995). The conduction bands correspond mostly to the Fe (3d)–and Fe (4s, 4p)–like orbitals. Unfortunately, the S (3d) and S (4s) orbitals play only a weak role in bonding, and for this reason, the sulfur L edge spectra show only weak features. It is possible to distinguish between sulfur as S_2^{2-} and $(SO_4)^{2-}$, but as will be shown below, the oxygen K edge spectra are much more sensitive to sulfate than are the sulfur L edge spectra; hence, the oxygen K edge spectra provide the most valuable information about the pyrite surface.

3.1.4. N K edge and Cl L edge spectra

Nitrogen K edge spectra revealed some nitrate adsorption, being more significant at high pH. There was no detectable chlorine edge for any sample, indicating that chloride is not an adsorbing species. The similarities (discussed below) between the oxidation products of pyrite samples exposed to nitrate and chloride ions, and also with samples conditioned only in deionized water, suggest that the background electrolyte was not

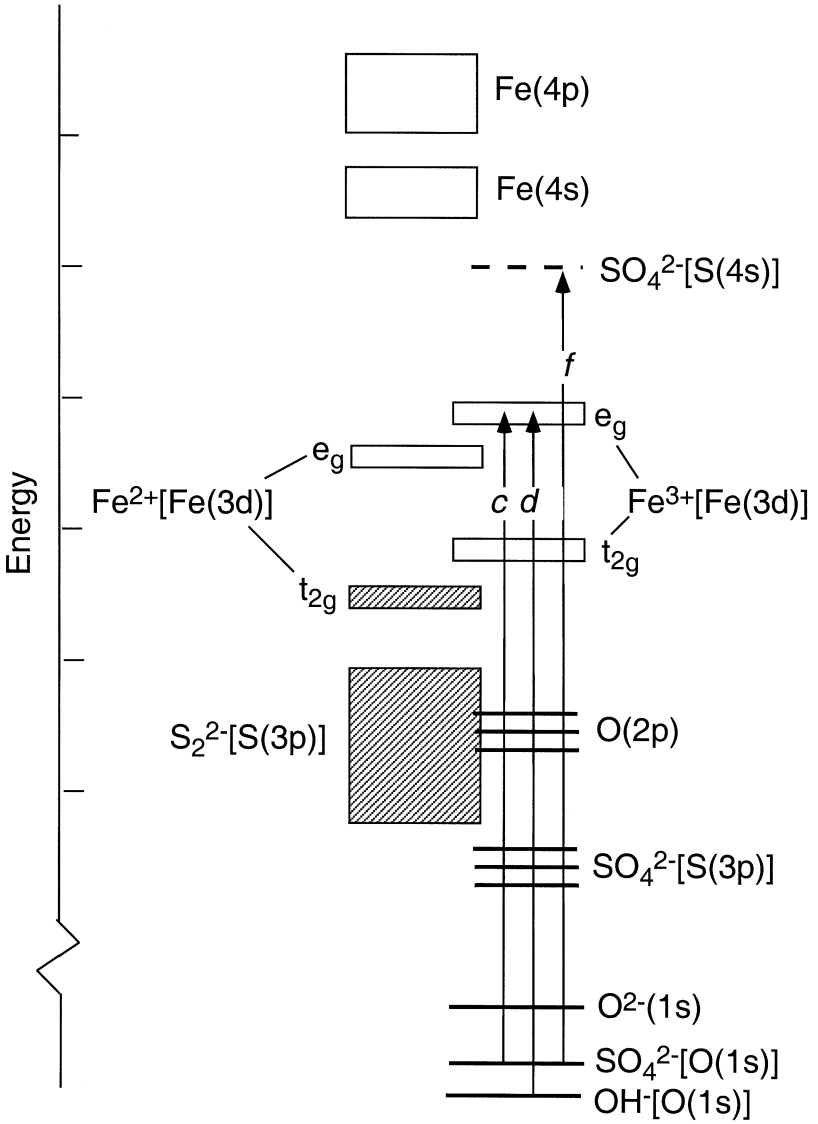

Fig. 4. Energy level diagram showing excitations corresponding to peaks in the O K edge spectrum of the oxidized pyrite surface.

having a direct effect on the nature of the oxidation products. Bonnissel-Gissinger et al. (1998) found in their experiments that NO_3^- did not oxidize the pyrite surface.

3.1.5. An electronic structure diagram for the oxidized pyrite surface

The relative energy positions of peaks in the X-ray absorption spectra for pyrite and its possible oxidation products were used to construct an electronic structure diagram for the oxidized pyrite surface (Fig. 4). Features in the O K edges in particular represent transitions between orbitals in the surface oxidation species and can be translated into the absolute energies of unoccupied states in the valence band. Knowledge of the electronic structure of the oxidized pyrite surface is crucial in understanding the redox behavior and passivation of the mineral in its natural environment.

3.2. Characterization of the Oxidized Pyrite Surface

3.2.1. Air-Saturated aqueous oxidation (with no additional Fe^{3+})

We find that the oxidation products of aqueous pyrite vary with pH. At low pH, the O K edge spectra of pyrite oxidized in both NaCl and $NaNO_3$ electrolytes (Figs. 5a and 6a) suggest that a ferric sulfate phase is the only surface oxidation product. In particular, the spectra of oxidized pyrite have a peak, f, at 537.2 eV, which is also found in ferric sulfate (Fig. 2c). As noted above, we assign this peak to the excitations occurring from the O (1s) level of oxygen in SO_4^{2-} to the S (4s)–O (2p) antibonding molecular orbital of sulfate (see Fig. 4). The peak is best resolved in the pyrite samples conditioned in sodium nitrate electrolyte (Fig. 5a). It can be seen at all pH values, but its relative intensity in the energy region above 535 eV appears

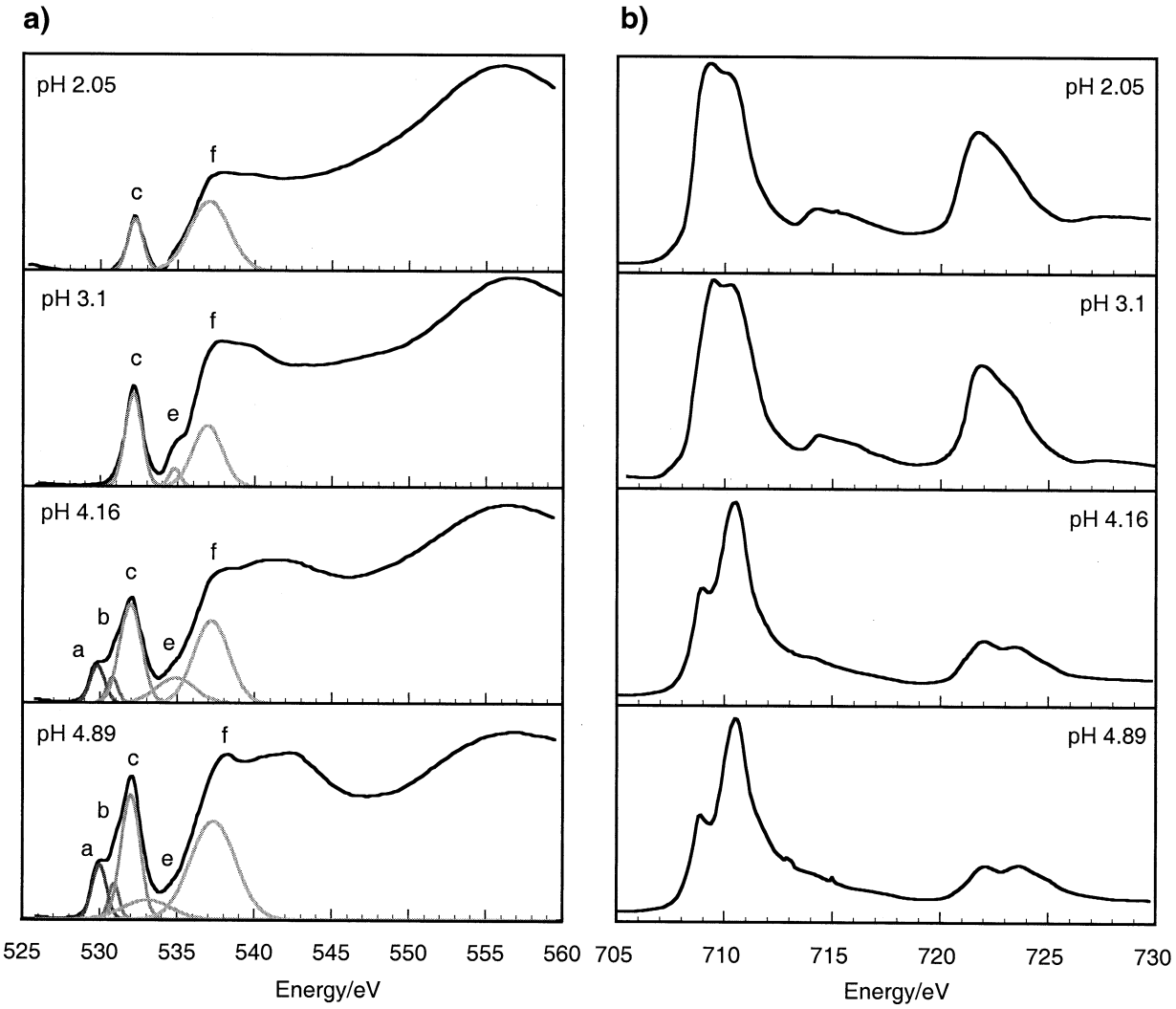

Fig. 5. (a) The oxygen K edges of a series of pyrite samples conditioned in $NaNO_3$ electrolyte at a range of pH. The spectra show a transition between pH 3 and 4, with a single peak, c, attributed to excitations from O (2p) states of oxygen in sulfate to an Fe (3d)–O (2p) state of ferric (hydroxy)sulfate, being replaced by additional peaks, a and b, at lower energy. The latter are attributed to excitations from O (2p) states of oxygen in oxide to Fe (III) t_{2g}- and e_g-like states of ferric iron as iron(III) oxyhydroxide becomes more stable with rising pH. (b) The iron L edges of a series of pyrite samples conditioned in $NaNO_3$ electrolyte at a range of pH. The spectra again show a marked transition at between pH 3 and 4, with peaks due to iron (II) in low-spin configuration being replaced by peaks due to iron (III) in high-spin configuration. This is interpreted to represent a transition, as the pH rises, from a mildly oxidized surface in which bulk pyritic iron (II) is the main iron species to a more extensively oxidized state in which iron(III) oxyhydroxide is the major product.

to decrease as the pH rises. The initial peak, c, at 532.2 eV is also seen in the ferric sulfate reference spectrum (Fig. 2c), although its intensity is somewhat reduced. This may indicate that there is an additional contribution from a hydroxy species, e.g., $Fe(OH)(SO_4)$, in the pyrite surface species. Natro-jarosite, $NaFe_3(SO_4)_2(OH)_6$, is a possible product, although it is unlikely to be stable across the entire pH range of the samples exhibiting peak c. Regardless of the precise nature of the surface product, the sulfate ion is the determining factor for the shape of the spectrum above 535 eV. Raman spectra of the sample conditioned in $NaNO_3$ electrolyte at pH 4.89 provide further evidence for sulfate species on the pyrite surface. Spectra taken of both a dark area on the pyrite surface and an acicular crystal visible within the pyrite sample (Fig. 7) show characteristic sulfate (Toniazzo et al., 1999) peaks at 800, 1025, and 1150 cm^{-1}.

The Fe L edges of the pyrite samples reacted in aqueous solutions (Figs. 5b and 6b) show that the surface iron is predominantly low-spin Fe(II) (as in FeS_2) at low pH. The L_{III}/L_{II} branching ratio of the iron spectrum is large for the samples conditioned below pH 4 compared to those at higher pH. There is some splitting of the Fe L edge, however, which suggests a small amount of Fe(III) in the surface. From the O K edge spectra (described above), we find that the ferric iron is present as a ferric (hydroxy)sulfate, not as an iron(III) oxyhydroxide. There is no evidence for oxygen bonded to high-spin Fe(II).

As the pH is increased to ~4, there is a marked change in

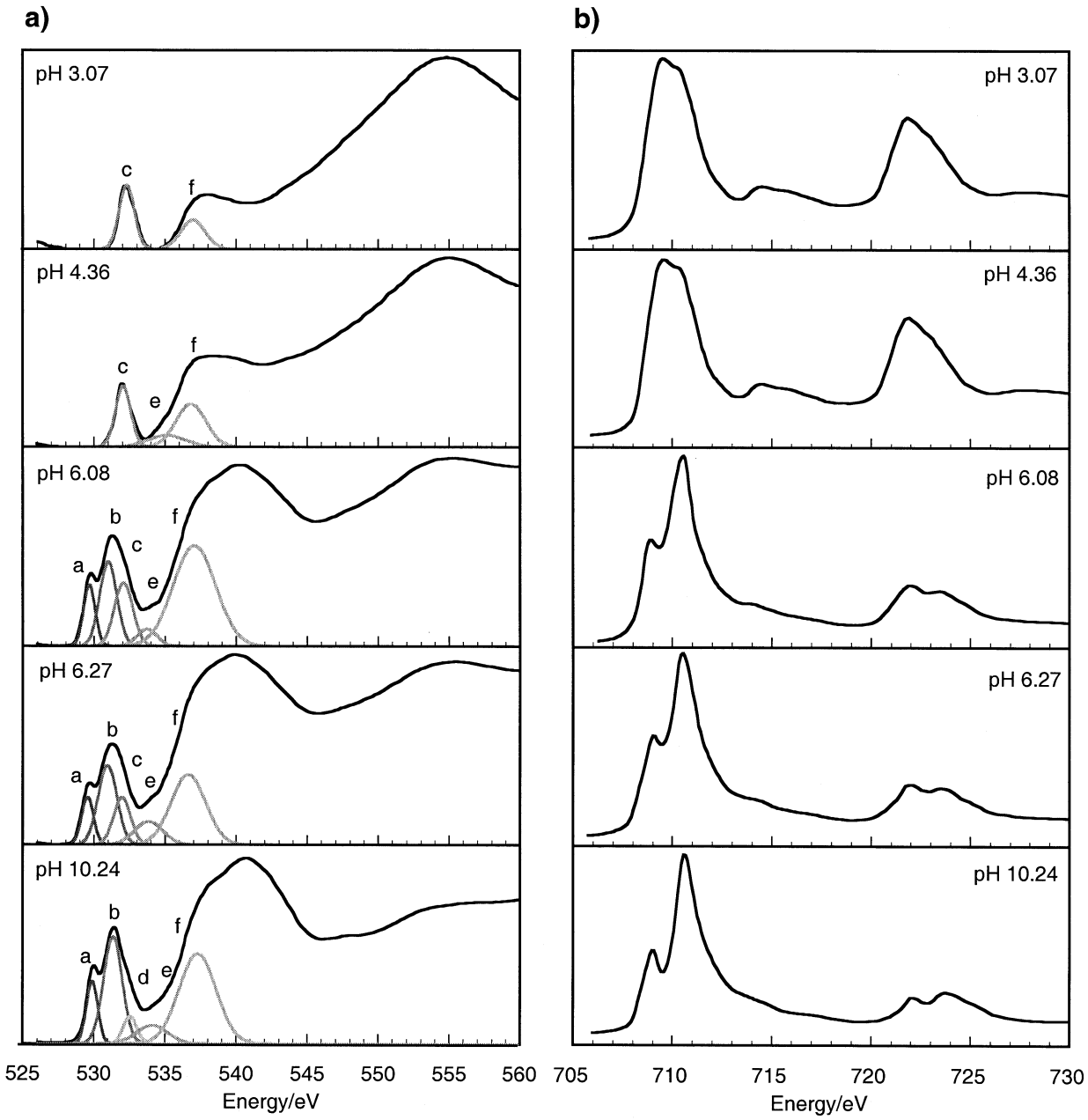

Fig. 6. (a) The oxygen K edges of a series of pyrite samples conditioned in NaCl electrolyte at a range of pH. The samples show the expected change from oxygen bonded to Fe(III) in a sulfate at low pH to oxygen bonded to Fe(III) in oxyhydroxide at higher pH. (b) The iron L edges of a series of pyrite samples conditioned in NaCl electrolyte at a range of pH. The samples show a pattern almost identical to that of those conditioned in $NaNO_3$ electrolyte, with iron (II) peaks being replaced by the split peaks characteristic of Fe (III) in octahedral coordination as the pH rises.

both the O K and Fe L edges, indicating the formation of a surface FeOOH phase. The oxygen spectrum exhibits two additional peaks, a and b, at low energy, which correspond to excitations to the Fe (3d) t_{2g}- and e_g-like states of octahedrally coordinated iron in an Fe(III)-O bond. The Fe L edge also mirrors this change, with the broad Fe(II) peak characteristic of the low-pH samples being replaced by the split peaks of Fe(III). These peaks are again attributed to the t_{2g}- and e_g-like states of Fe(III). The L_{III}/L_{II} branching ratio decreases, indicating a transition to a high-spin iron compound (Thole and Van der Laan, 1988). At the highest pH values (pH 10.24 for the sample conditioned in NaCl electrolyte), a peak, d, at 532.6 eV is present in the O K edge spectrum. This peak is assigned to excitations from the O (1s) level of OH^- to unoccupied Fe (3d) orbitals (see Fig. 4). The presence of peaks a, b, and d is diagnostic of an iron(III) oxyhydroxide surface species such as goethite.

The sulfur L edges (not shown) of the pyrite samples at higher pH are similar to those of the low-pH samples. Li et al. (1995) obtained the S L edge of pyrite after grinding in air and

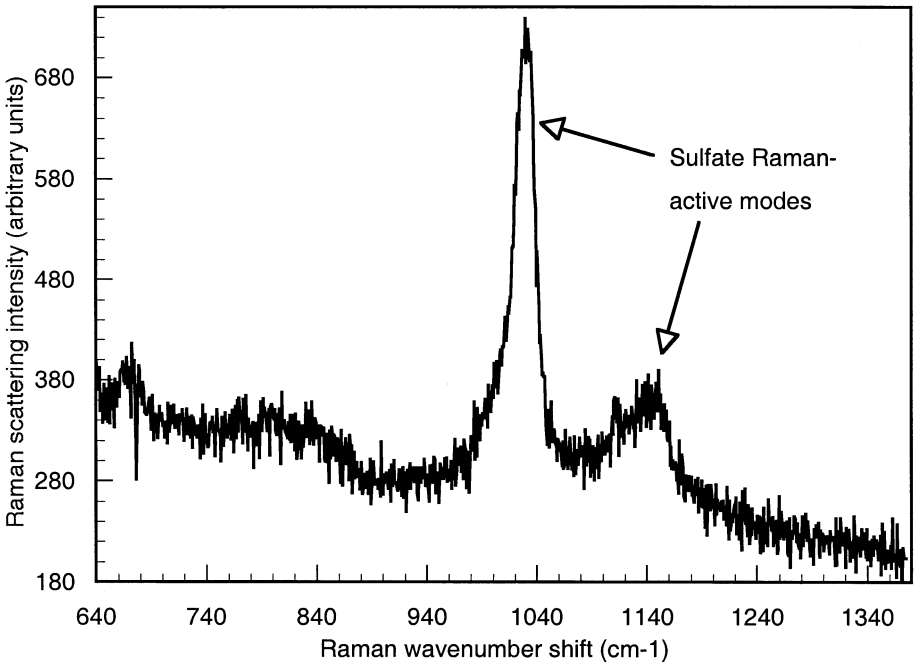

Fig. 7. Raman spectrum of pyrite conditioned in $NaNO_3$ electrolyte at pH 4.89. The spectrum shows peaks between 1000 and 1200 cm^{-1}, which correspond to sulfate Raman-active modes (Toniazzo et al., 1999).

suggested that the S_2^{2-} ion is the main feature in the electronic structure of pyrite. In this study, bulk disulfide indeed makes the dominant contribution in each case; however, there is an additional poorly resolved broad feature around 173.5 eV that we attribute to sulfate. This peak can also be observed in Mg, Ca, Sr, and Ba sulfates (Li et al., 1995) and is consistent with the previously discussed evidence for ferric (hydroxy)sulfate being the stable oxidation product of pyrite under acidic conditions, while iron(III) oxyhydroxides become more significant as the pH rises. At pH 10.24, for the sample conditioned in NaCl, pyrite can no longer be detected, and iron(III) oxyhydroxide is the dominant species to at least the 20- to 50-Å sampling depth probed (Abbate et al., 1992) using the TEY method.

The pyrite samples conditioned in different electrolytes show a very similar pattern of changing oxidation products (sulfate to oxyhydroxide) with pH. The Fe L edge, O K edge, and S L edge spectra all reflect the rising abundance of oxidation products and an increasing contribution of Fe(III) bonded to oxygen in oxyhydroxide at the expense of Fe(III) in a (hydroxy)sulfate. The results of Bonnissel-Gissinger et al. (1998) are consistent with those obtained here in that the $Fe2p_{3/2}$ XPS peak associated with iron(III) (hydr)oxides strongly increases as the pH of oxidation rises. Karthe et al. (1993) also observed that the ratio of Fe(III) to Fe(II) on the pyrite surface increases as pH rises, with Fe oxides failing to form below pH 4. Rosso et al (1999b) suggested that O_2- and H_2O-derived species react preferentially with Fe (3d) rather than S (3p) states but that S-O bonds may be formed eventually by hydrophilic attack to give sulfate precursors. The electronic structure of pyrite (Rosso et al., 1999a) is such that the highest occupied molecular orbitals (top of the valence band) are Fe (3d) character. We find here, however, that the initial surface oxidation product at low pH has both S-O bonds (as SO_4^{2-}) and Fe-O bonds. This may be due to rapid initial oxidation of monosulfide impurities, possibly followed by later oxidation of the disulfide component (Guevremont et al., 1998a).

3.3. Air-Saturated Aqueous Oxidation With Additional Fe^{3+}

The Fe L edge spectra of pyrite samples conditioned in a NaCl electrolyte with Fe^{3+} added to a concentration of 1.667×10^{-3} mol/L (Fig. 8b) show a different trend with rising pH than those of samples oxidized in the absence of ferric ions. Fe(III) is the dominant iron species on the pyrite surface at pH = 3 to 10, and the pyrite surface is significantly oxidized even under acidic conditions. The O K edges (Fig. 8a) reveal oxygen bonded to Fe(III) at all pH values, but there is evidence of a systematic change in the relative importance of the surface species. Peaks a and b, representing excitations from the oxygen (2p) level to the Fe (3d) t_{2g}- and e_g-like states of an Fe(III)-O bond, are present under all pH conditions. At low pH (2.87), peak c dominates the low-energy region of the spectrum, indicating the presence of a ferric (hydroxy)sulfate in addition to iron(III) oxyhydroxides. As the pH rises, however, the contribution from this species seems to decrease, and at pH 5.95, peak d at 532.5 eV, corresponding to excitations from the O (1s) level of oxygen in hydroxide, becomes important. Peak f, previously assigned to sulfate on the pyrite surface (see Table 1), also is more important under acidic conditions. At pH values greater than ~4, the major oxidation product is unambiguously an iron(III) oxyhydroxide, probably goethite. The sulfur L edges show no significant change over the pH range studied and reveal contributions mainly from the bulk disulfide structure along with minor sulfate. Fe sites appear to be the

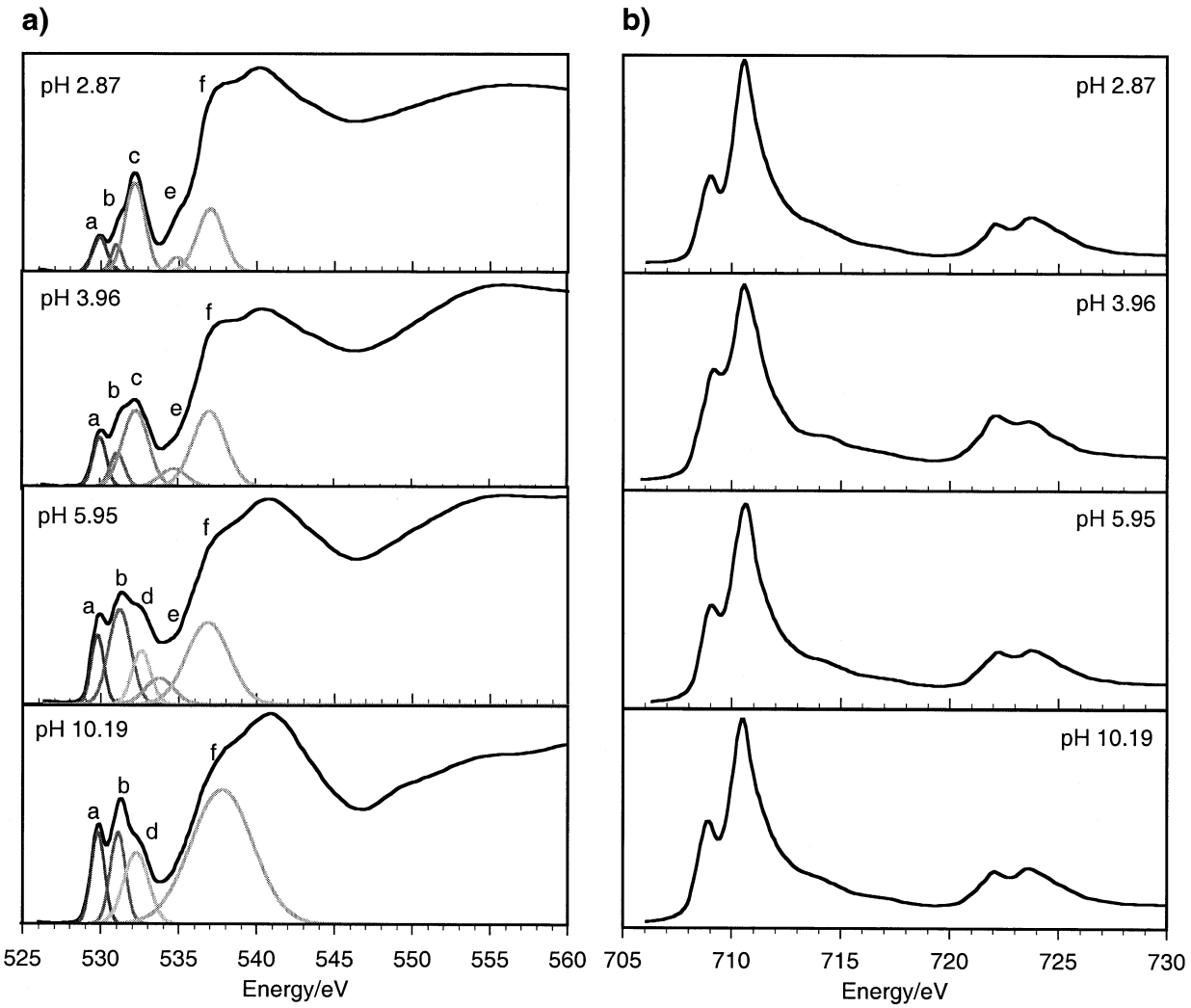

Fig. 8. (a) The oxygen K edges of a series of pyrite samples conditioned in NaCl electrolyte with added $FeCl_3$. The spectra indicate the presence of Fe(III) in all samples but show a systematic increase in the peak corresponding to excitations from the O (2p) level of oxygen in hydroxide, at the expense of the oxygen in sulfate. At pH 10, the oxidation product is unambiguously iron(III) oxyhydroxide, probably goethite. (b) The iron L edges of a series of pyrite samples conditioned in NaCl electrolyte with added $FeCl_3$. The spectra indicate the presence of Fe(III) and an extensively oxidized surface in all the samples, regardless of pH.

main loci for pyrite oxidation in the presence of additional aqueous ferric iron.

The apparent differences between the NaCl samples with and without additional ferric ions lend supporting evidence to previous observations that ferric ions catalyze the oxidation of pyrite (Moses and Herman, 1991). We find that iron(III) oxyhydroxide forms at more acid pH values in the presence of dissolved Fe^{3+}. It is likely that the rate of the oxidation reaction is accelerated by the presence of Fe^{3+}, and the formation of iron(III) oxyhydroxide, in addition to ferric (hydroxy)sulfate, is promoted. Fe^{3+} catalyzes pyrite oxidation by providing a conduit for electrons passing from pyrite to dissolved oxygen. Cyclic oxidation and reduction of adsorbed iron and the transfer of oxygen from the hydration sphere of the adsorbed Fe to the pyrite S continue until stable sulfoxy species dissociate from the surface (Moses and Herman, 1991).

3.4. Air Oxidation Products

Comparison of the aqueous samples to a sample oxidized in air reveals that the nature and/or relative proportions of different oxidation products of dry pyrite differ from those of aqueous pyrite. The air-oxidized sample has an oxygen K edge (Fig. 9a) almost identical to the ferric sulfate reference (Fig. 2c), with none of the additional peaks that complicate the aqueous samples.

The Fe L_{III} edge (Fig. 9b) is split into the peaks corresponding to excitations to the Fe (3d) t_{2g}- and e_g-like states of Fe(III), but it appears broadened and has a peak intensity ratio differing from that expected of a pure Fe(III) phase. As explained by Nesbitt et al. (1998) and Nesbitt and Muir (1994), contributions from surface Fe(III), as well as bulk and surface Fe(II), may explain the splitting and broad nature of the Fe L_{III} edge–

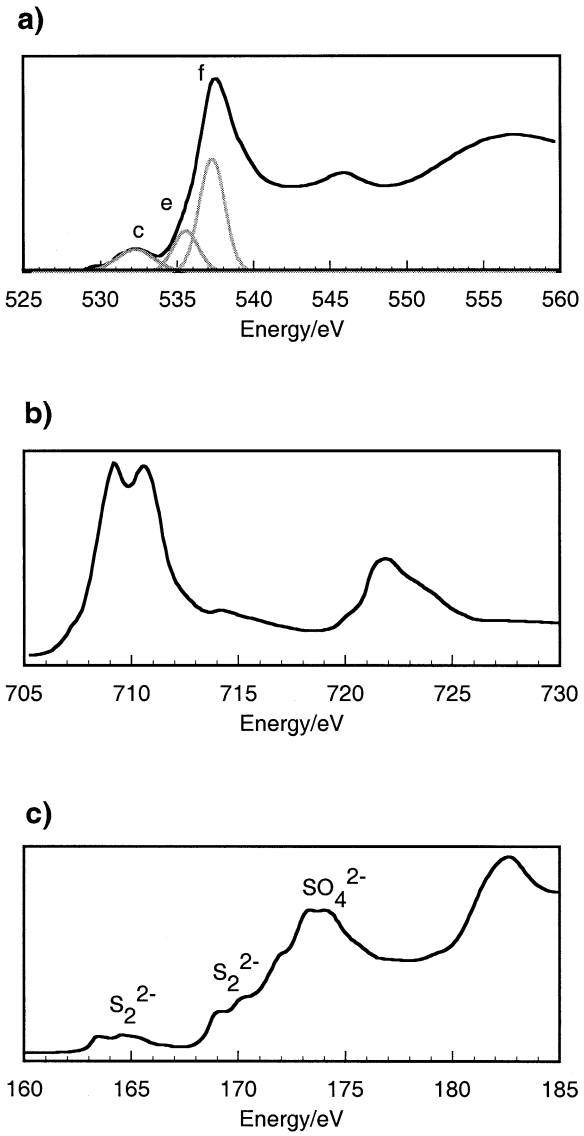

Fig. 9. (a) The oxygen K edge of pyrite oxidized in air. A peak, c, due to excitations to the iron 3d levels, is present at low energy, but the dominant feature, f, is caused by excitations from the oxygen (1s) level to S (4s) level of sulfur in sulfate. (b) The iron L edge of pyrite oxidized in air. The L_{III} edge shows the splitting of the 3d peak into the t_{2g}- and e_g-like levels, characteristic of iron(III). (c) The sulfur L edge of pyrite oxidized in air. The spectrum shows the typical peaks due to sampling of the bulk disulfide but also an additional prominent feature at higher energy. This is attributed to the presence of sulfate on the pyrite surface.

reflecting iron present in several oxidation states. It is thus proposed that on a fractured and oxidized pyrite surface, iron is present both as Fe(II) and Fe(III). The proportion of ferric iron may increase as the mineral is exposed to the oxidizing atmosphere for longer periods of time, with the surface eventually becoming completely passivated.

Finally, the sulfur L edge spectrum (Fig. 9c) confirms the presence of sulfate and supports the observations from the O K and Fe L edges. The bulk disulfide contribution is outweighed by strong peaks at 173.5 and 182.5 eV, which are due to sulfate. In this case, it can be inferred that the major oxidation product of pyrite under ambient conditions is ferric sulfate rather than iron(III) oxyhydroxide. This supports the results of Laajalehto et al. (1997) and Xu and Schoonen (1995), who invoked sulfate as the main oxidation product. The gaseous oxygen/water experiment of Guevremont et al. (1998a, 1998b), which produced sulfoxy (SO_2^{4-}), polysulfide groups, and thiosulfate, may be a good approximation for ambient atmospheric conditions, in which pyrite is exposed to significant concentrations of oxygen and water vapor at low temperatures. The S L and O K edges of the pyrite sample oxidized in air have much stronger sulfate contributions than those of the aqueous samples, although they contain the same peaks. This may be a function of the high aqueous solubility of ferric sulfate. Xu and Schoonen (1995) observed a rapid initial increase in sulfate concentration on addition of pyrite to an aqueous solution and attributed this to the dissolution of soluble sulfate salts on the surface. Fuhrmann et al. (1998) also suggested that the oxidation of pyritic sulfur is followed by its release into solution, while the oxidation of Fe results in formation of a new solid compound (FeOOH) on the surface. The X-ray spectra sample only the species on the mineral surface, while it is likely that the aqueous solutions also contain abundant oxidation products, particularly the soluble sulfur salts.

Pratesi and Cipriani (2000) and Nesbitt and Muir (1994) showed that the nature of sulfide alteration changes with the length of time the mineral is exposed to oxidizing environments. Pratesi and Cipriani (2000) proposed that O^{2-} and OH^- species become less significant with time, and SO_4^{2-} begins to dominate. Nesbitt et al. (2000), however, examined the surface species on a fractured pyrite surface and proposed that Fe-O species on pyrite develop slowly, requiring at least a few minutes to 24 h of exposure to air. Schaufuss et al. (1998) demonstrated that S^{2-} is by far the most reactive species on a fractured surface, with 80% being destroyed after 1 min exposure to air. S-O species are produced, indicating that sulfate is the initial oxidation product. Nesbitt et al. (2000) supplemented these findings by proposing that fracture of pyrite ruptures S-S bonds and produces S^{1-} moieties, which are reduced to S^{2-} with coincident auto-oxidation of Fe^{2+} to Fe^{3+}. This model is in best agreement with the results of the current study. Grinding or cleaving pyrite in air produces irregular fracture surfaces with Fe^{3+} and S^{2-} surface species. The sulfur dianion reacts rapidly with oxygen to produce sulfate, and surface iron reacts with oxygen and water to form iron(III) oxyhydroxide. It is possible that because pyrite is one of the more inert sulfide minerals, the air-oxidized surface experienced only the first stages of oxidation before insertion into the vacuum chamber. It would therefore be expected that sulfate is the major oxidation product of air-oxidized pyrite, with iron(III) oxyhydroxide forming as a subsidiary later phase.

4. CONCLUSIONS

Pyrite is reactive under ambient conditions and oxidizes rapidly in air to form a surface coating of ferric sulfate. The oxidation products of pyrite surfaces in aqueous solution vary with pH, with a marked transition occurring around pH 4. At low pH (2 to 4), the top 20 to 50 Å of pyrite surface is mostly FeS_2, with some ferric (hydroxy)sulfate present. At higher pH (4 to 7), iron(III) oxyhydroxide, in addition to ferric

(hydroxy)sulfate, constitute the top 20 to 50 Å, and there is no detectable FeS_2 remaining. Under alkaline conditions, the surface oxidation layer consists only of iron(III) oxyhydroxide (probably goethite). We find no evidence for hematite (α-Fe_2O_3) on the pyrite surface.

Acknowledgments—This work was made possible by direct access from the Central Laboratory of the Research Councils, Daresbury Laboratory, and the Natural Environment Research Council (NERC). E. C. Todd is supported by a NERC studentship. The authors would also like to thank J. M. Hayes and J. J. Wylde of the University of Bristol for their assistance with Raman spectroscopy. We are also grateful for the comments of three anonymous reviewers.

Associate editor: S. J. Traina

REFERENCES

Abbate M., Goedkoop J. B., de Groot F. M. F., Grioni M., Fuggle J. C., Hofmann S., Petersen H., and Sacchi M. (1992) Probing depth of soft-X-ray absorption-spectroscopy measured in total-electron-yield mode. *Surf. Interface Anal.* **18,** 65–69.

Bebie J., Schoonen M. A. A., Fuhrmann M., and Strongin D. R. (1998) Surface charge development on transition metal sulfides: An electrokinetic study. *Geochim. Cosmochim. Acta* **62,** 633–642.

Bianconi A., Dell'Ariccia M., Durham P. J., and Pendry J. B. (1982) Multiple scattering resonances and structural effects in the X-ray absorption near-edge spectra of Fe-II and Fe-III hexacyanide complexes. *Phys. Rev. B: Condens. Matter* **26,** 6502–6508.

Bonnissel-Gissinger P., Alnot M., Ehrhardt J. J., and Behra P. (1998) Surface oxidation of pyrite as a function of pH. *Env. Sci. Technol.* **32,** 2839–2845.

Brion D. (1980) Photoelectron spectroscopic study of the surface degradation of pyrite (FeS_2), chalcopyrite ($CuFeS_2$), sphalerite (ZnS), and galena (PbS) in air and water. *Appl. Surf. Sci.* **5,** 133–152.

Bronold M., Tomm Y., and Jaegermann W. (1994) Surface states on cubic d-band semiconductor pyrite (FeS_2). *Surf. Sci. Lett.* **314,** L931–L936.

Buckley A. N. and Woods R. (1987) The surface oxidation of pyrite. *Appl. Surf. Sci.* **27,** 437–452.

Chen J. G. (1997) NEXAFS investigations of transition metal oxides, nitrides, carbides and sulfides and other interstitial compounds. *Surf. Sci. Rep.* **30,** 1–152.

de Groot F. M. F., Grioni M., Fuggle J. C., Ghijsen J., Sawatzky G. A., and Petersen H. (1989) Oxygen 1s X-ray-absorption edges of transition-metal oxides. *Phys. Rev. B: Condens. Matter* **40** (8), 5715–5723.

Dekkers M. J. and Schoonen M. A. A. (1994) An electrokinetic study of synthetic greigite and pyrrhotite. *Geochim. Cosmochim. Acta* **58,** 4147–4153.

Eggleston C. M., Ehrhardt J. J., and Stumm W. (1996) Surface structural controls on pyrite oxidation kinetics: An XPS-UPS, STM and modeling study. *Am. Mineral.* **81,** 1036–1056.

Fornasiero D., Eijt V., and Ralston J. (1992) An electrokinetic study of pyrite oxidation. *Colloids Surf.* **62,** 63–73.

Fuhrmann M., Bajt S., and Schoonen M. A. A. (1998) Sorption of iodine on minerals investigated by X-ray absorption near edge structure (XANES) and ^{125}I tracer experiments. *Appl. Geochem.* **13,** 127–141.

Goldhaber M. B. (1983) Experimental study of metastable sulfur oxyanion formation during pyrite oxidation at pH 6-9 and 30°C. *Am. J. Sci.* **283,** 193–217.

Guevremont J. M., Bebie J., Elsetinow A. R., Strongin D. R., and Schoonen M. A. A. (1998a) Reactivity of the (100) plane of pyrite in oxidizing gaseous and aqueous environments: Effects of surface imperfections. *Env. Sci. Technol.* **32,** 3743–3748.

Guevremont J. M., Elsetinow A. R., Strongin D. R., Bebie J., and Schoonen M. A. A. (1998b) Structure sensitivity of pyrite oxidation: Comparison of the (100) plane and (111) planes. *Am. Mineral.* **83,** 1353–1356.

Hyland M. M. and Bancroft G. M. (1989) An XPS study of gold deposition at low-temperatures on sulfide minerals—Reducing agents. *Geochim. Cosmochim. Acta* **53,** 367–372.

Karthe S., Szargan R., and Suoninen E. (1993) Oxidation of pyrite surfaces: A photoelectron spectroscopic study. *Appl. Surf. Sci.* **72,** 157–170.

Kurata H., Lefevre E., Colliex C., and Brydson R. (1993) Electron-energy-loss near-edge structures in the oxygen K-edge spectra of transition-metal oxides. *Phys. Rev. B: Condens. Matter* **47** (20), 13763–13768.

Laajalehto K., Kartio I., and Suoninen E. (1997) XPS and SR-XPS techniques applied to sulfide mineral surfaces. *Int. J. Mineral. Proc.* **51,** 163–170.

Li D., Bancroft G. M., Kasrai M., Fleet M. E., Feng X. H., and Tan K. H. (1995) S K-edge and L-edge X-ray-absorption spectroscopy of metal sulfides and sulfates—Applications in mineralogy and geochemistry. *Can. Mineral.* **33,** 949–960.

McIntyre N. S. and Zetaruk D. G. (1975) X-ray photoelectron spectroscopic studies of iron oxides. *Anal. Chem.* **49**(11), 1521–1529.

McKibben M. A. and Barnes H. L. (1986) Oxidation of pyrite in low temperature acidic solutions: Rate laws and surface textures. *Geochim. Cosmochim. Acta* **50,** 1509–1520.

Moses C. O. and Herman J. S. (1991) Pyrite oxidation at circumneutral pH. *Geochim. Cosmochim. Acta* **55,** 471–482.

Moses C. O., Nordstrom D. K., Herman J. S., and Mills A. L. (1987) Aqueous pyrite oxidation by dissolved oxygen and by ferric iron. *Geochim. Cosmochim. Acta* **51,** 1561–1571.

Mycroft J. R., Bancroft G. M., Mcintyre N. S., Lorimer J. W., and Hill I. R. (1990) Detection of sulfur and polysulfides on electrochemically oxidized pyrite surfaces by X-ray photoelectron spectroscopy and Raman spectroscopy. *J. Electroanal. Chem.* **292,** 139–152.

Mythen C. S., Van der Laan G., and Padmore H. A. (1992) The undulator beamline at the SRS Daresbury. *Rev. Sci. Instrum.* **63** (1), 1313–1316.

Nesbitt H. W. and Muir I. J. (1994) X-ray photoelectron spectroscopic study of a pristine pyrite surface reacted with water vapor and air. *Geochim. Cosmochim. Acta* **58,** 4667–4679.

Nesbitt H. W., Bancroft G. M., Pratt A. R., and Scaini M. J. (1998) Sulfur and iron states on fractured pyrite surfaces. *Am. Mineral.* **83,** 1067–1076.

Nesbitt H. W., Scaini M., Hochst H., Bancroft G. M., Schaufuss A. G., and Szargan R. (2000) Synchrotron XPS evidence for Fe^{2+}-S and Fe^{3+}-S surface species on pyrite fracture surfaces, and their 3d electronic states. *Am. Mineral.* **85,** 850–857.

Nicholson R. V., Gillham R. W., and Reardon E. J. (1988) Pyrite oxidation in carbonate-buffered solution: 1. Experimental kinetics. *Geochim. Cosmochim. Acta* **52,** 1077–1085.

Nicholson R. V., Gillham R. W., and Reardon E. J. (1990) Pyrite oxidation in carbonate-buffered solution: 2. Rate control by oxide coatings. *Geochim. Cosmochim. Acta* **54,** 395–402.

Pratesi G. and Cipriani C. (2000) Selective depth analyses of alteration products of bornite, chalcopyrite and pyrite performed by XPS, AES, RBS. *Eur. J. Mineral.* **12,** 397–409.

Rosso K. M., Becker U., and Hochella M. F. Jr. (1999a) Atomically resolved electronic structure of pyrite {100} surfaces: An experimental and theoretical investigation with implications for reactivity. *Am. Mineral.* **84,** 1535–1548.

Rosso K. M., Becker U., and Hochella M. F. Jr. (1999b) The interaction of pyrite (100) surfaces with O_2 and H_2O: Fundamental oxidation mechanisms. *Am. Mineral.* **84,** 1549–1561.

Schaufuss A. G., Nesbitt H. W., Kartio I., Laajalehto K., Bancroft G. M., and Szargan R. (1998) Reactivity of surface chemical states on fractured pyrite. *Surf. Sci.* **411,** 321–328.

Sherman D. M. (1985a) The electronic structures of Fe^{3+} coordination sites in iron oxides: Applications to spectra, bonding and magnetism. *Phys. Chem. Miner.* **12,** 161–175.

Sherman D. M. (1985b) SCF-Xα-SW study of Fe-O and Fe-OH chemical bonds: Applications to the Mossbauer spectra and magneto chemistry of hydroxyl-bearing iron oxides and silicates. *Phys. Chem. Miner.* **12,** 311–314.

Sherman D. M. and Waite T. D. (1985) Electronic spectra of Fe^{3+} oxides and oxide hydroxides in the near-IR to near-UV. *Am. Mineral.* **70,** 1262–1269.

Sparrow T. G., Williams B. G., Rao C. N. R., and Thomas J. M. (1984) L_3/L_2 white-line intensity ratios in the electron energy-loss spectra of 3d transition metal oxides. *Chem. Phys. Lett.* **108** (6), 547–550.

Sugiura C. (1981) Sulfur K- X-ray absorption-spectra of FeS, FeS_2 and Fe_2S_3. *J. Chem. Phys.* **74,** 215–217.

Sugiura C. (1984) Iron K- X-ray absorption-edge structures of FeS and FeS_2. *J. Chem. Phys.* **80,** 1047–1049.

Sugiura C. and Muramatsu S. (1985) Sulfur K- X-ray absorption-edge structures and electronic states of transition-metal sulfides MS and MS_2 (M = Fe, Co, Ni). *Phys. Status Solidi B* **129,** K157–K161.

Toniazzo V., Mustin C., Portal J. M., Humbert B., Benoit R., and Erre R. (1999) Elemental sulfur at the pyrite surfaces: Speciation and quantification. *Appl. Surf. Sci.* **143,** 229–237.

Thole B. T. and Van der Laan G. (1988) Branching ratio in X-ray absorption-spectroscopy. *Phys. Rev. B: Condens. Matter* **38,** 3158–3171.

Xu Y. and Schoonen M. A. A. (1995) The stability of thiosulfate in the presence of pyrite in low-temperature aqueous solutions. *Geochim. Cosmochim. Acta* **59,** 4605–4622.